Conformation-resolved UV spectra of Pb(II) complexes: A gas phase study of the sandwich structures [Pb(toluene)$_2$]$^{2+}$ and [Pb(benzene)$_2$]$^{2+}$

Lifu Ma, Tsukiko Takashima, Joseph Koka, Helen J. Kimber, Hazel Cox, and Anthony J. Stace

View Online   Export Citation   CrossMark

AIP
Publishing
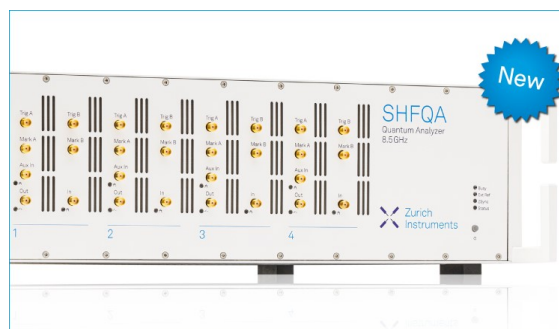
Conformation-resolved UV spectra of Pb(II) complexes: A gas phase study of the sandwich structures [Pb(toluene)₂]²⁺ and [Pb(benzene)₂]²⁺

Lifu Ma,[1] Tsukiko Takashima,[2] Joseph Koka,[1] Helen J. Kimber,[2] Hazel Cox,[2,a)] and Anthony J. Stace[1,a)]

[1]*School of Chemistry, University of Nottingham, University Park, Nottingham NG7 2RD, United Kingdom*
[2]*Department of Chemistry, University of Sussex, Falmer, Brighton BN1 9QJ, United Kingdom*

Toxic heavy metals, such as Pb^{2+}, have become important targets for the development of efficient receptors that are capable of recognizing their presence as environmental and biological pollutants, and an important part of that receptor–metal characterization process is the provision of spectral evidence that identifies the presence of a metal ion. From results reported here on a combined experimental and theoretical study it is shown that, when complexed with aromatic ligands, Pb^{2+} is capable of yielding structured UV spectra, which: (i) exhibit discrete electronic transitions that include significant contributions from the metal ion; (ii) are very sensitive to the electronic properties of coordinating ligands; and (iii) are sensitive to subtle changes in coordination geometry. Two aromatic sandwich complexes, [Pb(benzene)₂]²⁺ and [Pb(toluene)₂]²⁺ have been prepared in the gas phase and their UV action spectra recorded from ions held and cooled in an ion trap. Whilst [Pb(benzene)₂]²⁺ exhibits a spectrum with very little detail, that recorded for [Pb(toluene)₂]²⁺ reveals a rich structure in the wavelength range 220–280 nm. Theory in the form of density functional theory (DFT) shows that both types of complex take the form of hemidirected structures, and that [Pb(toluene)₂]²⁺ can adopt three distinct conformers depending upon the relative positions of the two methyl groups. Further calculations, using adiabatic time-dependent DFT to assign electronic transitions, provide evidence of individual [Pb(toluene)₂]²⁺ conformers having been resolved in the experimental spectrum. Of particular significance for the development of methods for identifying Pb^{2+} as an environmental or biological pollutant, is the observation that there are distinct ligand-to-metal charge transfer transitions in the UV that are sensitive to both the geometry and the electronic characteristics of molecules that accommodate the metal ion. © *2013 AIP Publishing LLC*. [http://dx.doi.org/10.1063/1.4801440]

INTRODUCTION

The selective binding of heavy metal ions, such as Pb^{2+}, to sequestering agents has proved to be an effective mechanism for trapping and identifying their presence under a wide range of circumstances.[1–7] In the environment, the goal is to minimise the consequences of both natural and man-made lead pollution;[1–5,7,8] in biological systems, the objectives are to detect the presence of Pb^{2+} and to understand the mechanism behind the metal's toxicity.[6,9–13] In almost all cases, spectroscopy is a key tool for detecting the presence of the dication in terms of the influence Pb^{2+} has on either the direct absorption of radiation[3–5,8–10] or on fluorescent emission.[14] In order to quantify the effects acquisition of Pb^{2+} can have on the structural and electronic properties of molecules, a study has been made of the UV spectra of two simple aromatic systems where the metal can form strongly bound sandwich structures. Whilst many of the proposed sequestering agents are aromatic,[1,2,4,8] it is recognized that the metal ion will occupy a wide range of very different sites. However, because active Ligand-to-Metal Charge Transfer (LMCT) transitions in the UV are going to provide important signatures for the metal, evidence of how sensitive such transitions are to site

and geometry could make a significant contribution to the development of effective sequestering agents.

UV-visible spectroscopy is routinely used to investigate energy level differences between electronic states of metal complexes in the condensed phase either in solution or when isolated in a matrix.[15] Under both circumstances, broadening and the perturbation of transition energies due to the presence of a solvent frequently cause problems which comparable studies in the gas phase can be expected to minimize or eliminate completely. However, many experiments on the gas phase spectroscopy of metal complexes have concentrated on singly charged ions, and a large catalogue of such studies now exists at both infrared and UV-visible wavelengths.[16] Since the most common charge state for many metals is +2, it would seem important to develop techniques where dication complexes can also be studied under conditions where the influence of both solvent and counterion can be eliminated. However, there are clear technical reasons as to why there have been so few such studies;[17] the most obvious being the difficulty in preparing a range of complexes and once formed, their tendency to undergo charge transfer. Despite these problems, there have been a number of very successful experiments on metal dication complexes.[18,19] Stace, Cox, and co-workers[20] have reported state-resolved UV photofragmentation spectra for [Zn(pyridine)₄]²⁺, [Mn(pyridine)₄]²⁺,[21]

a)Electronic addresses: h.cox@sussex.ac.uk and a.j.stace@nottingham.ac.uk

and a series of Group 2 metal-pyridine and metal-picoline complexes,[22] all of which were recorded using the pick-up technique in conjunction with a cold ion trap. Apart from the open-shell $[Mn(pyridine)_4]^{2+}$ complex,[21] quantitative assignments of the spectra have been possible from density functional theory (DFT) and time-dependent DFT (TDDFT) calculations.[20,22] At longer wavelengths, Williams and co-workers[23–25] have successfully used a combination of electrospray and multiphoton IR excitation to record spectra from a range of doubly charged metal ion/water complexes, and tunable infrared radiation has also been used to investigate the structures of complexes formed between alkaline earth ions and small molecules of biological significance.[26–28]

To date, all studies of the spectroscopy of Pb(II) complexes have been undertaken in the condensed phase,[29] with many of the experiments focusing on the identification and characterisation of suitable sequestering agents.[1,3] Bauer and co-workers[30] recorded Raman spectra for a series of complexes containing closed-shell metal ions, including Pb(II), both in the solid state and in solution ($CHCl_3$ or CH_2Cl_2) for the purposes of tracking changes that occur in metal ion coordination in different environments. Other studies at UV/visible wavelengths have either been mostly theoretical or have combined theory with measurements made in the condensed phase. Zhang and co-workers[3,31] have used TDDFT to calculate electronic absorption and circular dichroism spectra of Pb(II)/phthalocyanine complexes over a wavelength range that overlaps with the work presented here. Cornard and co-workers[4,8,32,33] have reported the results of a series of TDDFT calculations on the electronic spectra of numerous Pb(II) chellate complexes involving aromatic molecules. For complexes involving both hydroxyflavone molecules and chlorogenic acid, no prominent charge transfer transitions involving the metal ion were identified.[4,8] In contrast, both Pb(II)-caffeate and Pb(II)-quercetin complexes showed evidence of spectral features that could be attributed to ligand-metal-charge transfer transitions.[32,33] Jarzęcki[10] has presented the results of a detailed TDDFT study of electronic excitations in lead-poisoned model proteins for comparison with experimental data. Of relevance to the work presented here, the calculations identified the presence of a number of ligand-to-metal charge transfer transitions at between 200 and 230 nm.[10]

Reported here are the first spectroscopic results of a gas phase study where Pb(II) has been complexed with benzene and toluene as ligands to form sandwich structures with the general form $[Pb(benzene)_2]^{2+}$ and $[Pb(toluene)_2]^{2+}$. The experimental data are compared with the results of DFT and TDDFT calculations and from the latter it has been possible to assign the main features that appear in the UV spectra.

EXPERIMENT

A detailed description of the apparatus has been given in Ref. 18. Briefly, argon carrier gas at a pressure of 2 bars has been passed through either benzene or toluene held in an ice-cooled reservoir. The resultant mixed vapour was allowed to expand through a 50 μm diameter nozzle before passing through a 1 mm diameter skimmer. The collimated beam of mixed argon/solvent clusters then passed over a Knudsen cell

containing pieces of lead heated to a temperature that was sufficient to generate a metal vapour pressure of between 10^{-3} and 10^{-2} mbar. At this controlled temperature, a balance could be established between there being sufficient metal vapour for the effective pick up of atoms by the mixed clusters, the need to avoid scattering the molecular beam, and the contents of the crucible lasting the duration of a typical spectral scan ($\sim$45 h). Previous experiments have shown the pick-up technique to be capable of forming a wide range of stable complexes between Pb^{2+} and a variety of molecular ligands,[34] and to generate stable ion signals from the complexes $[Pb(toluene)_2]^{2+}$ and $[Pb(benzene)_2]^{2+}$, the temperature of the Knudsen cell varied between 790 °C and 890 °C.

Neutral lead/molecule complexes passed into the ion source of a quadrupole mass spectrometer (Extrel) where they were ionised by high energy electron impact (100 eV). From a mixture of ions present in the source, each of the $[Pb(L)_2]^{2+}$ complexes (L = benzene or toluene) was mass selected with a quadrupole mass filter, and steered by quadrupole deflector into an ion guide where they were transmitted to a quadrupole Paul ion trap. The end caps of the latter were grounded and continuously cooled through a jacket that was attached to an external reservoir filled with liquid nitrogen. Helium buffer gas (5×10^{-4} mbar) contained within the trap was cooled by collisions with the cold surfaces, and over a total trapping time of 1.2 s, collisions between the helium and trapped ions led to a considerable reduction in the internal energy content of the latter. Based on the observation of unimolecular decay by trapped ions, their internal temperature was thought to drop from >500 K to somewhere in the range 100–150 K. Compared with previous examples of metal dication spectra,[19,35] this cooling procedure has led to the appearance of discrete structure in spectra which, in turn, has made a valuable contribution to the assignment of transitions.[20–22] The walls of the chamber housing the trap are baked continuously to reduce the water content of the background gas (see below). In the absence of either an ion beam or buffer gas, the base pressure in the chamber was 1×10^{-8} mbar.

An electronic gate in front of ion trap opened for 300 ms at the start of each trapping cycle and then shut for 900 ms to allow the ions to cool and undergo photoexcitation. The trapped ions were exposed to seven 10 ns pulses of tunable UV radiation from a frequency-doubled, Nd:YAG pumped dye laser. Subsequently, all precursor and photofragment ions were ejected from the trap by ramping the RF voltage on the ring electrode. A channeltron detector located behind one of the end caps recorded ion signals, which were then averaged for 200 trap cycles, each lasting 1200 ms. An advantage of using the quadrupole trap is that ions with all values of m/z were swept out and detected at the end of each trap cycle. Spectra were calculated as

$$Photofragment\ yield$$
$$= \frac{\sum photofragment\ intensities}{\sum photofragment\ intensities + precursor\ ion\ intensity}$$

(1)

and normalised with respect to variations in laser and precursor ion intensity.

THEORY

The structures and binding energies of $[Pb(benzene)_2]^{2+}$, $[Pb(benzene)]^{+/2+}$, $[Pb(toluene)_2]^{2+}$, and $[Pb(toluene)]^{+/2+}$, were calculated using density functional theory as implemented in GAUSSIAN 09.[36] Geometry optimization and frequency analysis were performed using the local density approximation (LDA)[37] together with the gradient-corrected exchange of Becke[38] and the correlation correction of Perdew[39] (BVP86). Structural minima were verified by the absence of imaginary vibrational modes. These calculations were compared with results calculated using the meta-hybrid functional of Tao, Perdew, Staroverov, and Scuseria (TPSSh)[40] and the Adamo hybrid functional of Perdew, Burke, and Ernzerhof (PBE1PBE, known as PBE0 in the literature).[41] A 6-311++G(d,p) basis set was used for all atoms except Pb^{2+}, for which the standard SDD relativistic pseudopotential, ECP78MWB, was used.[42] This will be referred to as 6-311++G(d,p)[SDD] throughout the text. All energies presented are zero point energy corrected.

Excitation energies and oscillator strengths were calculated using TDDFT with the optimized structures calculated using each of the methodologies outlined above (viz., BVP86, TPSSh, and PBE0). The SCF step of TDDFT was performed using the long-range corrected hybrid exchange-correlation functional CAM-B3LYP (Coulomb-Attenuating Method B3LYP),[43] PBE0 and TPSSh. For the purposes of identifying the contribution each orbital makes to an electronic transition, the dominant transitions predicted by TDDFT were analyzed by calculating the natural transition orbitals (NTOs).[44] The results obtained were qualitatively similar and so only the CAM-B3LYP excitations at the BVP86 geometry are presented as this methodology provided the best overall agreement with experiment; comparison data from the other methods can be found in the supplementary material.[45]

RESULTS AND DISCUSSION

Experimental UV photofragment spectra

The signal corresponding to $[Pb(benzene)_2]^{2+}$ at m/z 181.5 was first optimised through the trap onto a channeltron detector with the ring electrode RF signal switched off. With the RF on a 1200 ms duty cycle of trapping, laser excitation and ejection was initiated to record and average over 200 cycles. An example of a typical photofragment mass spectrum is shown in Figure 1 where there are three clearly distinguishable peaks on a m/z scale that has been calibrated using the known masses of cluster ions. The spectrum shows two parent ion peaks which are identified as $[Pb(benzene)_2]^{2+}$ and $[Pb(benzene)_2H_2O]^{2+}$ and one fragment peak corresponding to $C_6H_6^+$. No other fragments were observed. The precursor ion, $[Pb(benzene)_2]^{2+}$, appears to readily pick up a water molecule from the background gas. In previous studies of the spectra of $[ML_4]^{2+}$ complexes,[20–22] other precursor dications were also observed to pick up water molecules; however, calculations showed that their presence had very little influence on the recorded UV spectra.[22] In addition, the extent of water attachment was found to decline as the ion trap
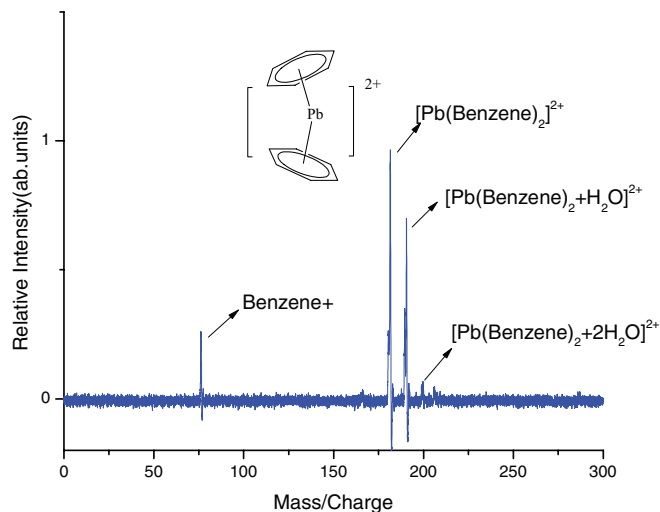

FIG. 1. Example of a photofragment mass spectrum for $[Pb(benzene)_2]^{2+}$ recorded after trapping and irradiation at $45\,355$ cm^{-1}. Also shown is the structure calculated for this ion.

cooled and any background water was removed via cryo-umping. The intensities of the precursors and fragment ions from mass spectra were monitored simultaneously to record a photofragment yield at each step in UV wavelength. A complete UV photofragmentation spectrum for $[Pb(benzene)_2]^{2+}$ is shown in Figure 2, which has been constructed by combining the yield/photon energy plots from multiple scans with a range of laser dyes, and fitted together by averaging in regions of overlap between adjacent scans. From Figure 2, it can be seen that the spectrum consists of three main features: two well-resolved peaks at $39\,800$ cm^{-1} and $42\,000$ cm^{-1}, and a very broad feature which extends beyond the upper limit of the photon energy range available from the laser $\sim\!45\,500$ cm^{-1}.

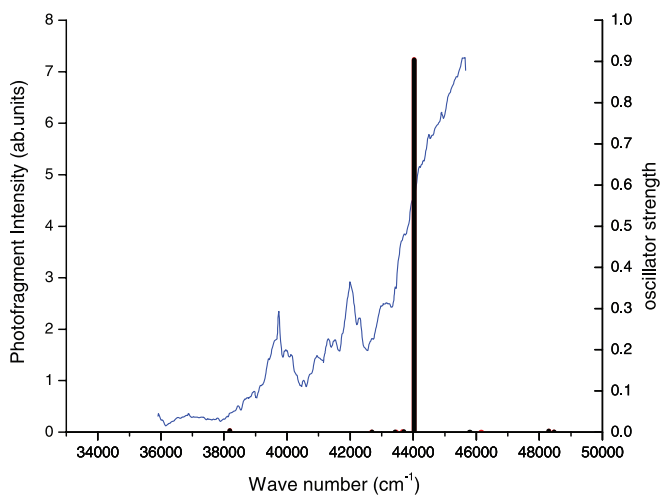FIG. 2. UV photofragment spectrum recorded for $[Pb(benzene)_2]^{2+}$ overlaid with electronic excitations where the energies and oscillator strengths have been calculated using TDDFT (CAM-B3LYP/6-311++G(d,p)[SDD] at BVP86 geometry). The calculated transitions are shown as vertical lines and are for two conformers (C_2 and C_{2v}) of $[Pb(benzene)_2]^{2+}$; however, on the scale of the plot the individual transitions are not resolved.

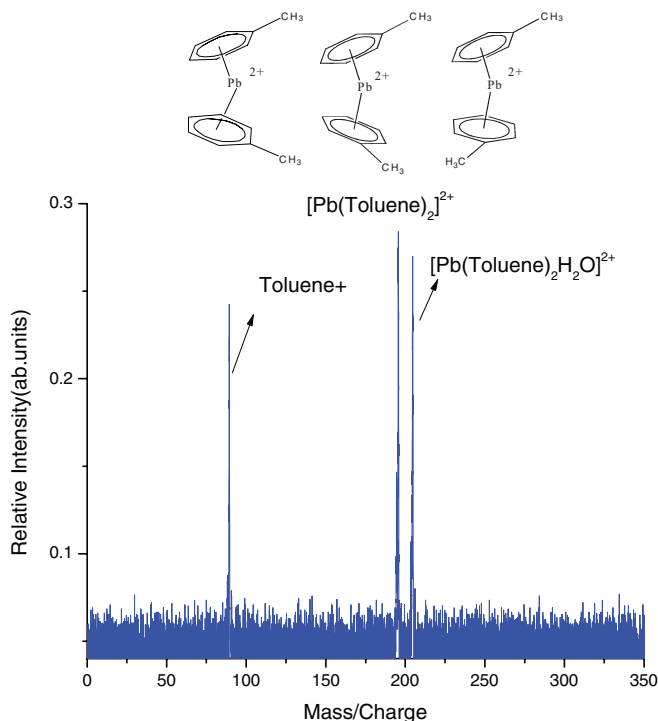FIG. 3. Example of a photofragmentation mass spectrum for $[Pb(toluene)_2]^{2+}$ recorded after trapping and irradiation at 42 135 cm^{-1}. Also shown are the three separate conformations of $[Pb(toluene)_2]^{2+}$ which calculations suggest may be present in the experiment.
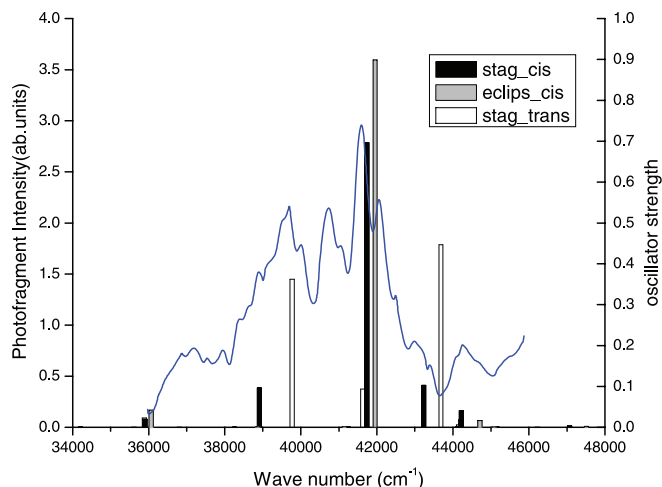

FIG. 4. UV photofragment spectrum recorded for $[Pb(toluene)_2]^{2+}$ overlaid with electronic excitations where the energies and oscillator strengths have been calculated using TDDFT (CAM-B3LYP/6-311++G(d,p)[SDD] at BVP86 geometry). Results calculated for the three separate conformations of $[Pb(toluene)_2]^{2+}$ are shown as vertical lines.

An example of a photofragmentation mass spectrum recorded for $[Pb(toluene)_2]^{2+}$ at m/z = 195.5 is shown in Figure 3. As with $[Pb(benzene)_2]^{2+}$, there are two clearly identifiable peaks relating to $[Pb(toluene)_2]^{2+}$ and $[Pb(toluene)_2H_2O]^{2+}$ ions, together with one fragment peak corresponding to $C_7H_8^+$. As can be seen, $[Pb(toluene)_2]^{2+}$ also exhibits a tendency to pick up water molecules from the background gas. A combined UV photofragmentation spectrum is shown in Figure 4 where it can be seen that there are a number of resolved features in a spectrum that is very different from that recorded for $[Pb(benzene)_2]^{2+}$. The $[Pb(toluene)_2]^{2+}$ spectrum consists of five dominant features appearing at: 37 000, 39 700, 40 700, 41 600, and 44 300 cm^{-1}. There is also a resolved peak at 42 000 cm^{-1} which resides close to a prominent feature at 41 600 cm^{-1}.

Since photoexcitation of the dications, $[Pb(benzene)_2]^{2+}$ and $[Pb(toluene)_2]^{2+}$, leads to the appearance of single identifiable photofragments, namely, $C_6H_6^+$ and $C_7H_8^+$, respectively, features common to the two dications will be discussed in terms of generic ions and their fragments, namely, $[Pb(X)_2]^{2+}$, $[PbX]^+$, and X^+. Tables I and II provide details of calculated binding energies with respect to (i) complete neutral loss, defined as $[PbX_2]^{2+} \rightarrow Pb^{2+} + 2X$; (ii) charge transfer, defined as $[PbX_2]^{2+} \rightarrow [PbX]^+ + X^+$; and (iii) incremental neutral loss, defined as $[PbX_2]^{2+} \rightarrow [PbX]^{2+} + X$, where X is either benzene or toluene. The loss of a single neutral ligand (X) can be achieved at the photon energies used in these experiments, but the loss of two ligands cannot. Likewise, the formation of X^+ is thermodynamically possible, but no allowance is made for the energy required to access the excited state that would lead to this ion. However, it is quite possible that a crossing to such a state will fall below the ~1.4 eV reverse Coulomb barrier; the two singly charged fragments will encounter as they begin to separate, in which case a route to the appearance of X^+ can be identified.

TABLE I. Binding energies for the $[Pb(benzene)_2]^{2+}$ complex with respect to various loss products and calculated using both BVP86/6-311++G(d,p)[SDD] and TPSSh/6-311++G(d,p)[SDD].

		Energy (kJ mol^{-1})	
Reaction	$[Pb(Bz)_2]^{2+}$	BVP86	TPSSh[a]
$[Pb(Bz)_2]^{2+} \rightarrow Pb^{2+} + 2 \,(Bz)$	$^1A_1$ (C_{2v}: Eclipsed)	645.0	638.2
	^1A (C_2: Staggered)	644.8	638.2
$[Pb(Bz)_2]^{2+} \rightarrow [Pb(Bz)]^+ + (Bz)^+$	$^1A_1$ (C_{2v}: Eclipsed)	24.2	22.5
	^1A (C_2: Staggered)	24.1	22.4
$[Pb(Bz)_2]^{2+} \rightarrow [Pb(Bz)]^{2+} + (Bz)$	$^1A_1$ (C_{2v}: Eclipsed)	191.6	192.4
	^1A (C_2: Staggered)	191.5	192.3

[a]The TPSSh staggered geometry lowered the symmetry to C_S.

TABLE II. Binding energies for the $[Pb(toluene)_2]^{2+}$ complex with respect to various loss products and calculated using both BVP86/6-311++G(d,p)[SDD] and TPSSh/6-311++G(d,p)[SDD].

		Energy (kJ mol^{-1})	
Reaction	$[Pb(tol)_2]^{2+}$	BVP86	TPSSh
$[Pb(tol)_2]^{2+} \rightarrow Pb^{2+} + 2\,(tol)$	$^1A_1$ (C_{2v}: Eclipsed-cis)	692.1	682.7
	^1A (C_2: Staggered-cis)	692.0	682.6
	^1A (C_2: Staggered-trans)	692.0	682.7
$[Pb(tol)_2]^{2+} \rightarrow [Pb(tol)]^+ + (tol)^+$	$^1A_1$ (C_{2v}: Eclipsed-cis)	8.8	9.8
	^1A (C_2: Staggered-cis)	8.7	9.7
	^1A (C_2: Staggered-trans)	8.7	9.7
$[Pb(tol)_2]^{2+} \rightarrow [Pb(tol)]^{2+} + (tol)$	$^1A_1$ (C_{2v}: Eclipsed-cis)	197.5	198.1
	^1A (C_2: Staggered-cis)	197.4	198.0
	^1A (C_2: Staggered-trans)	197.4	198.1

Structure calculations

Calculations show all of the $[Pb(benzene)_2]^{2+}$ and $[Pb(toluene)_2]^{2+}$ conformers to be bent, i.e., the rings of the sandwich complexes are not parallel, but have a centroid-Pb-centroid angle of $\sim162°$ rather than $180°$. The staggered and eclipsed parallel structures of the $[Pb(benzene)_2]^{2+}$ complex, with symmetries D_{6d} and D_{6h}, respectively, are stationary states, characterized by a large imaginary mode, which when distorted, results in the bent analogues, with symmetries C_2 (staggered) and C_{2v} (eclipsed), respectively. A pictorial image of a $[Pb(benzene)_2]^{2+}$ structure is shown in Figure 1. Similarly, the $[Pb(toluene)_2]^{2+}$ complexes are calculated to have either staggered rings (C_2 symmetry) or eclipsed rings (C_{2v} symmetry). However, due to the methyl group, there is an additional staggered conformation depending on the relative orientation of the methyl groups (i.e., cis or trans). The 3 minima identified will be referred to as:[46] (i) eclipsed-cis, (ii) staggered-cis, and (iii) staggered-trans and pictorial images of the three structures are shown in Figure 3. Pb(II) complexes are often found to be hemi-directed,[29,47] i.e., the Pb-ligand bonds are directed towards just part of the coordination sphere, and so it is possible that the calculated structures seen here are of a similar nature. The hemi-directed character of Pb(II) complexes has been attributed to an "inert pair effect" where relativistic contributions cause the Pb(II) $6s^2$ orbital to contract.[29,47] The $[Pb(benzene)]^{2+}$ complex is essentially η^6 as expected, whereas $[Pb(toluene)]^{2+}$ and $[Pb(benzene)]^+$ are both closer to η^1 with approximate C_s symmetry (i.e., the shortest Pb–C distance involves the para-carbon of toluene). The $[Pb(toluene)]^+$ complex is also η^1 but in this case the

Pb ion sits over the meta-carbon. It is clear from the data in Tables I and II that the $[PbX_2]^{2+}$ conformers for both complexes are extremely close in energy (within 1 kJ mol^{-1}) and so they are all expected to be present in the ion trap. Structural data for all complexes are provided in the supplementary material.[45]

TDDFT calculation of spectra

Excitation energies and oscillator strengths for both the C_2 (staggered) and C_{2v} (eclipsed) structures of the $[Pb(benzene)_2]^{2+}$ complex are given in Table III and plotted as stick spectra together with the experimental results in Figure 2. No transitions were calculated to occur below 37 000 cm^{-1} and both conformers give just a single very strong LMCT (oscillator strength, $f = 0.9$) electronic transition, and these are predicted to occur at 43 243 cm^{-1} (staggered) and 43 276 cm^{-1} (eclipsed). There are also a number of much weaker transitions ($f < 0.002$) calculated to occur within the range of the experiment. Figure 5 shows the NTO orbitals that are involved in the two configurations that give rise to the transition at 43 276 cm^{-1}; these configurations are representative of many of the other LMCT transitions that are calculated to be present. The experimental results (Figure 2) yield a single broad spectral feature above 43 000 cm^{-1}, and although the transitions calculated for the two conformers fall in this region they alone cannot be assigned to this feature.

Furthermore, the calculations fail to match the two relatively small features seen at 39 800 and 42 000 cm^{-1} in the experimental spectrum. To investigate further the origin(s) of these additional features, excitation energies and

TABLE III. Summary of calculated TDDFT electronic transitions and their intensities ($f \geq 0.01$) for $[Pb(benzene)_2]^{2+}$ and $[Pb(benzene)]^{2+}$. The weight and character of the dominant configurations and the % Pb character are also given.

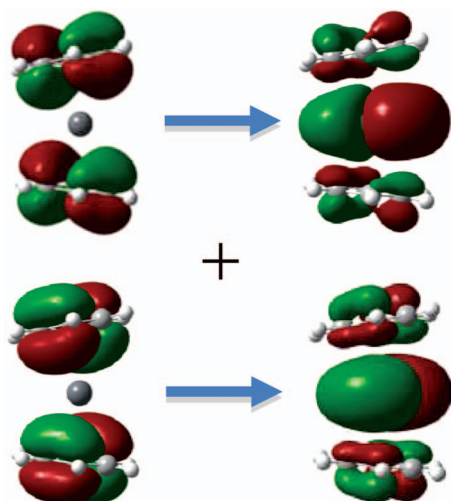| Structure	Calculated transition energy (cm^{-1})	Oscillator strength, f	NTO description	Assignment
$[Pb(Bz)_2]^{2+}$				
C_2 (staggered)	43 243	0.936	LMCT (51%) + LMCT (46%)	LMCT $\pi \rightarrow 6p$ ($> 95\%$ Pb)
C_{2v} (eclipsed)	43 276	0.932	LMCT (52%) + LMCT (45%)	LMCT $\pi \rightarrow 6p$ ($> 95\%$ Pb)
$Pb(Bz)^{2+}$	50 656	0.319	(LM)MCT (46%) (LM)MCT (46%)	LMCT $\pi + 6p$ (10%) $\rightarrow 6p$ (93% Pb)

FIG. 5. Configurations involved in the dominant electronic excitation of C_{2v} [Pb(benzene)$_2$]$^{2+}$. This ligand-to-metal ($\pi \rightarrow 6p$) charge transfer transition is representative of other LMCT transitions. The lead atom is depicted at the centre of the structure as a grey sphere.
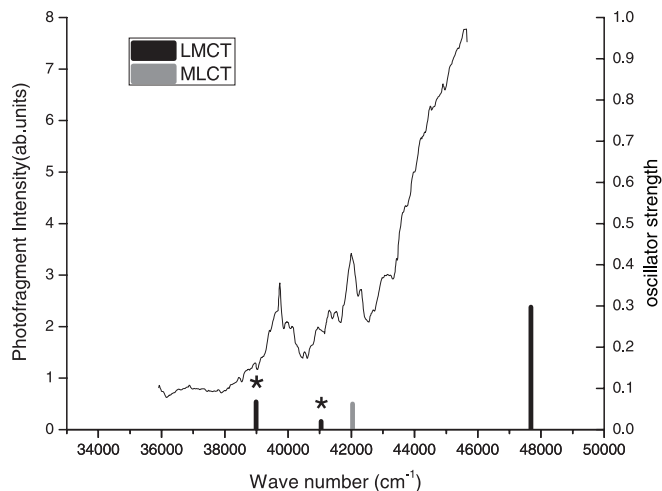

FIG. 6. UV photofragment spectrum recorded for [Pb(benzene)$_2$]$^{2+}$ overlaid with electronic excitations calculated for [Pb(benzene)]$^+$ using TDDFT (CAM-B3LYP/6-311++G(d,p)[SDD] at BVP86 geometry). The calculated results are shown as vertical lines. The transitions identified by * are subject to spin contamination.

oscillator strengths were calculated for the [Pb(benzene)]$^+$ complex, which could act as a transient on the route to the appearance of $C_6H_6^+$. These results are given in Table IV and are plotted as stick spectra against the experimental data in Figure 6. There are four calculated electronic transitions in the experimental range (with $f \geq 0.01$), and they are a good match with some of the features that appear in the experimental spectrum that is also shown in Figure 6. Furthermore, three of the excitations are LMCT which could yield $C_6H_6^+$ as a photofragment. The level of agreement between the experimental and calculated results suggests that some fraction of the $C_6H_6^+$ photofragment yield originates from [Pb(benzene)]$^+$, which in turn is a product of the photofragmentation of [Pb(benzene)$_2$]$^{2+}$. However, it can be seen from Table IV that two of the electronic transitions calculated for [Pb(benzene)]$^+$ have associated with them a significant degree of spin contamination, which means there is some uncertainty over their validity. (See the Appendix for further information.) In addition, it should be noted that the recorded experimental spectrum will be a convolution of the individual contributions attributed to [Pb(benzene)$_2$]$^{2+}$ and [Pb(benzene)]$^+$.

The excitation energies and oscillator strengths calculated for the three structures identified for [Pb(toluene)$_2$]$^{2+}$ are summarised in Table V and plotted as stick spectra against the experimental photofragment spectrum in Figure 4. From their assignments, it can be seen that the three optimized structures yield a total of seven dominant ($f > 0.05$) LMCT transitions; those predicted to occur at 39 016 and 39 663 cm^{-1} are in good agreement with the substantial peak occurring at ~39 700 cm^{-1}, and two intense LMCT transitions predicted for 41 844 and 41 955 cm^{-1} show good agreement with the large features at 41 600 cm^{-1} and 42 000 cm^{-1} in the experimental spectrum. A cluster of excitations involving configuration mixing of LMCT and $\pi^* \leftarrow \pi$ (LLCT) transitions from 44 095 to 44 708 cm^{-1} is in good agreement with the relatively small feature observed at 44 300 cm^{-1}, and the calculations could also account for the weak feature seen at approximately 37 000 cm^{-1}. However, there is no match from the calculations for the experimental result seen at 40 700 cm^{-1}.

Since the dominant photofragment observed following the excitation of [Pb(toluene)$_2$]$^{2+}$ is toluene$^+$, steps

TABLE IV. Summary of the observed peak positions and the calculated TDDFT (CAM-B3LYP/6-311++G(d,p)[SDD] at BVP86 geometry) electronic transitions and oscillator strengths ($f \geq 0.01$ in the experimental range 35 000–45 000 cm^{-1}) for [Pb(benzene)]$^+$. The weight and character of the dominant configuration for each spin and the % Pb character are also given as are $\langle \widehat{S}^2 \rangle$ values, which should be 0.75 in the absence of contamination.

Peak positions (cm^{-1})					
Observed	Calculated	Oscillator strength, f	$\langle \widehat{S}^2 \rangle$	NTO description	Assignment
39 800	38 990	0.067	1.00	α-LMCT (49%)	LMCT
				β-LMCT (110%)	$\pi \rightarrow 6p$ (> 80% Pb)
	41 050	0.020	1.89	α-LMCT (69%)	LMCT
				β-LMCT (89%)	$\pi \rightarrow 6p$ (> 64% Pb)
42 000	42 038	0.062	0.77	α-MLCT (196%)	MLCT
					$6p$ (94% Pb)$\rightarrow \sigma^* + s$ (12% Pb)
~45 500	47 680	0.297	0.76	α-LMCT (78%)	LMCT
				β-LMCT (85%)	$\pi \rightarrow 6p$ (> 66% Pb)

TABLE V. Summary of the observed peak positions and the calculated TDDFT (CAM-B3LYP/6-311++G(d,p)[SDD] at BVP86 geometry) electronic transitions and oscillator strengths ($f \geq 0.01$ in the experimental range 35 000–45 000 cm^{-1}) for [Pb(toluene)$_2$]$^{2+}$. The weight and character of the two most dominant configurations and % Pb character are also given. Dominant transitions from both theory and experiment, are shown in bold.

Peak positions (cm^{-1})		Oscillator strength, f	NTO description	Assignment[a]
Observed	Calculated[a]			
	35 778[b]	0.023	LMCT (64%) + LMCT (35%)	LMCT $\pi \to 6p$ (> 88% Pb)
36 873	36 012[c]	0.020	LMCT (63%) + LMCT (36%)	LMCT $\pi \to 6p$ (> 88% Pb)
37 000	36 062[d]	0.042	LMCT (70%) + LMCT (29%)	LMCT $\pi \to 6p$ (> 88% Pb)
39 700	39 016[c]	0.096	(LM)MCT (90%)	(LM)MCT $\pi + 6p$ (11%) $\to 6p$ (92% Pb)
	39 663[b]	**0.363**	**LMCT 51%) + LMCT (47%)**	**LMCT $\pi \to 6p$ (> 86% Pb)**
40 700	41 516[b]	0.094	LMCT (62%) + (LM)MCT (37%)	LMCT $\pi \to 6p$ (92% Pb) (LM)MCT $\pi + 6p$ (12%) $\to 6p$ (92% Pb)
41 600	**41 844[c]**	**0.696**	**LMCT (63%) + LMCT (34%)**	**LMCT $\pi \to 6p$ (> 90% Pb)**
42 000	**41 955[d]**	**0.899**	**LMCT (69%) + LMCT (28%)**	**LMCT $\pi \to 6p$ (> 90% Pb)**
43 000	43 342[c]	0.103	(LM)MCT (56%) 10% Pb $\to$ 78% Pb + LLCT (19%)	(LM)MCT $\pi + 6p$ (10%) $\to 6p$ (78% Pb) LLCT $\pi \to \pi^a$
	43 576[b]	**0.447**	**LMCT (72%) +LMCT (23%)**	**LMCT $\pi \to 6p$ (> 78% Pb)**
44 300	44 095[b]	0.018	L(LM)CT (36%) + LLCT (36%)	L(LM)CT $\pi \to \pi^a + 6p$ (13% Pb) LLCT $\pi \to \pi^a$
	44 328[c]	0.040	LMCT (46%) 86% Pb + LLCT (25%)	LMCT $\pi \to 6p$ (86% Pb) LLCT $\pi \to \pi^a$
	44 708[d]	0.017	(LM)MCT (40%) + LLCT (30%)	(LM)MCT $\pi + 6p$ (12%) $\to 6p$ (86% Pb) LLCT $\pi \to \pi^a$

[a]The states arising from the C$_2$ staggered (cis and trans) structures are of ^{1}B symmetry. The states arising from the C$_{2v}$ eclipsed structure are of ^{1}B$_1$ or ^{1}B$_2$ symmetry.
[b](Stag-trans).
[c](Stag-cis).
[d](Eclips-cis).

were taken to see if photoexcitation of the intermediate [Pb(toluene)]$^+$ contributes to the spectrum given in Figure 4. TDDFT calculations on [Pb(toluene)]$^+$ were undertaken using the same level of theory as before and these results are summarized in Table VI and plotted in Figure 7 together with the experimental spectrum. Six dominant transitions ($f \geq 0.01$) are calculated to reside within the energy range of the experimental spectrum; however, the oscillator strengths are much lower than those calculated for electronic transitions in [Pb(toluene)$_2$]$^{2+}$. Five of the transitions in [Pb(toluene)]$^+$ can be assigned predominantly to LMCT, and the strong transition at 41 111 cm^{-1} is a metal-to-ligand charge transfer (MLCT) transition, which is a close match to the unassigned feature observed at 40 700 cm^{-1}; however, it should be noted that, unlike the case for [Pb(benzene)]$^+$ the experimental result being assigned to [Pb(toluene)]$^+$ is comparable in intensity to those assigned to [Pb(toluene)$_2$]$^{2+}$. The transition at

41 111 cm^{-1} is not spin contaminated and can be considered reliable, however, it should be noted that a number of other electronic transitions calculated for [Pb(toluene)]$^+$ have associated with them a significant degree of spin contamination and hence there is uncertainty over their validity (see the Appendix). Similar to [Pb(benzene)$_2$]$^{2+}$, it would appear that at least one feature in the photofragmentation spectrum of [Pb(toluene)$_2$]$^{2+}$ could be attributed to the presence of a transient intermediate, which the trap is unable to capture.

Photofragmentation mechanism

The above calculations have identified contributions to the UV photofragmentation spectra of both dications that could arise from singly and doubly charged lead-containing ions. Taking this observation together with the fact that the

TABLE VI. Summary of the observed peak positions and the calculated TDDFT (CAM-B3LYP/6-311++G(d,p)[SDD] at BVP86 geometry) electronic transitions and oscillator strengths ($f \geq 0.01$ in the experimental range 35 000–45 000 cm^{-1}) for [Pb(toluene)]$^+$. The weight and character of the dominant configuration for each spin and the % Pb character are also given as are $\langle \widehat{S}^2 \rangle$ values, which should be 0.75 in the absence of contamination. The most dominant transitions, from theory or experiment, are shown in bold.

Peak positions (cm^{-1})					
Observed	Calculated	Oscillator strength, f	$\langle \widehat{S}^2 \rangle$	NTO description	Assignment
…	35 244	0.022	1.03	α-LMCT (94%) β-LMCT (79%)	LMCT $\pi \rightarrow 6p$ (> 57% Pb)
37 000	**38 098**	**0.066**	1.04	α-LMCT (45%) β-LMCT (109%)	LMCT $\pi \rightarrow 6p$ (> 70% Pb)
39 700	39 663	0.027	1.69	α-LMCT (68%) β-LMCT (115%)	**LMCT** $\pi \rightarrow 6p$ (> 63% Pb)
40 700	**41 111**	**0.065**	0.77	α-MLCT (196%)	**MLCT** $6p$ (93% Pb)$\rightarrow \sigma* + s$ (13% Pb)
41 600					
44 300	44 517	0.038	1.31	α-LMCT (62%) β-LMCT (66%)	LMCT $\pi \rightarrow 6p$ (> 73% Pb)
	44 966	0.019	2.14	α-L(LM)CT (36%) β-LMCT (106%)	L(LM)CT $\pi \rightarrow \pi* + 6p$ (25% Pb) LMCT $\pi \rightarrow 6p$ (63% Pb)
Outside range	**47 397**	**0.157**	0.77	α-LMCT (72%) β-LMCT (82%)	**LMCT** $\pi \rightarrow 6p$ (> 61% Pb)

photofragment mass spectra for both complexes display just a single non-metallic fragment, two possible mechanisms are discussed. Both capable of generating the product ions of interest and these are
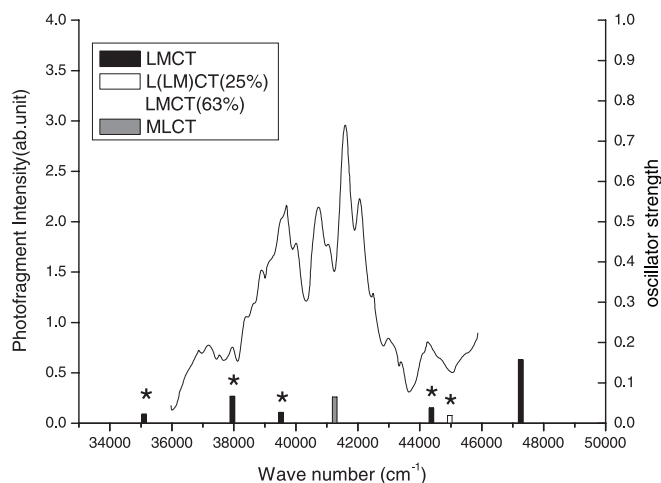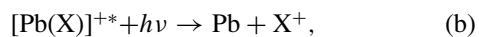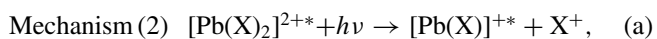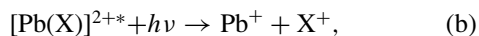
Mechanism (1) $[Pb(X)_2]^{2+*} + h\nu \rightarrow [Pb(X)]^{2+*} + X$,   (a)

$[Pb(X)]^{2+*} + h\nu \rightarrow Pb^+ + X^+$,   (b)

Mechanism (2) $[Pb(X)_2]^{2+*} + h\nu \rightarrow [Pb(X)]^{+*} + X^+$,   (a)

$[Pb(X)]^{+*} + h\nu \rightarrow Pb + X^+$,   (b)
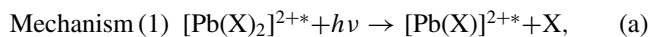

FIG. 7. UV photofragment spectrum recorded for [Pb(toluene)$_2$]$^{2+}$ overlaid with electronic excitations calculated for [Pb(toluene)]$^+$ using TDDFT (CAM-B3LYP/6-311++G(d,p)[SDD] at BVP86 geometry). The calculated results are shown as vertical lines and note that the scales are the same as those used in Figure 4. The transitions identified by * are subject to spin contamination.

where * denotes an ion in an excited state, which can be either an electronic state or the ground state, but with extensive vibrational excitation. Each mechanism is capable of generating X$^+$, which is the only photofragment to be observed (Figures 1 and 3). An earlier study of the formation and fragmentation of Pb^{2+} complexes failed to observe [Pb(benzene)]$^{2+}$,[34] which would suggest that this complex is unstable and that the second step in mechanism (1) should be spontaneous following the loss of neutral benzene from [Pb(benzene)$_2$]$^{2+}$. That being the case, then Pb$^+$ should be observed in the trap. However, charge transfer followed by Coulomb explosion will release up to 1.8 eV of kinetic energy and the corresponding momentum of Pb$^+$ could be sufficiently high that the very light helium containment gas is unable to quench and confine the ion to the trap. Previous experiments have shown the trapping efficiency for metal complexes to be extremely sensitive to ion kinetic energy.[18] For mechanism (2), the second step might be expected to yield Pb$^+$ rather than X$^+$ because the lead atom has a lower first ionization energy (IE(Pb) = 7.42 eV and IE(benzene) = 9.24 eV, IE(toluene) = 8.83 eV). Mechanism (2) could operate if Pb(X)$^{+*}$ fragmented from an electronic excited state that correlated with X$^+$ as a reaction fragment, and the spectra calculated for both [Pb(benzene)]$^+$ and [Pb(toluene)]$^+$ certainly provide evidence of charge transfer transitions. A charge transfer step of this nature has been observed following the photoexcitation of singly charged [Pb(benzene)]$^+$ and [Pb(benzene)$_2$]$^+$ complexes at visible wavelengths.[48] Contributions from [Pb(X)]$^+$ to the photofragment spectrum could come from this ion should it remain in the trap during each laser cycle. As mentioned above, one reason why heavy singly charged fragments from Coulomb explosion may not be observed in the mass spectra is that they acquire sufficient momentum that they cannot be contained in the trap by collisions with the very much lighter helium gas. Since Coulomb

explosion occurs on a $\sim 10^{-13}$ s timescale it is possible that, as the [Pb(benzene)]$^+$ fragment passes through the trap it remains susceptible to photofragmentation from the residual photons in each 5 ns laser pulse.

Either mechanism will only work if Coulomb fission imparts sufficient momentum to the metal-containing fragment that it cannot be contained within the trap. Mechanism (1) provides the most obvious route to the appearance of X$^+$ as the principal photofragment; however, the match between calculated and experimental spectra provides evidence for the presence of [Pb(X)]$^+$ ions at some point in the photoexcitation cycle. That being the case, then mechanism (2) in association with a charge transfer transition in step (b) must also make a contribution.

CONCLUSION

A combination of theory and experiment has been used to identify the origins of features recorded in the UV electronic spectra of two Pb(II) sandwich complexes, namely, [Pb(benzene)$_2$]$^{2+}$ and [Pb(toluene)$_2$]$^{2+}$. For the benzene complex, TDDFT calculations show that the single most intense feature recorded at $\sim 45\,500$ cm^{-1} in the experimental spectrum is due to a $\pi \rightarrow$ Pb (6p) LMCT transition. In contrast, the [Pb(toluene)$_2$]$^{2+}$ complex has a far richer UV spectrum and TDDFT results indicate that it includes contributions from three distinct (almost isoenergetic) conformers. However, all of the dominant spectral features arising from this complex can again be attributed to LMCT transitions, although as the wavelength decreases $\pi \rightarrow \pi^*$ transitions via configuration mixing contribute to the spectra.

Of relevance with regard to the development of methods for sequestering and identifying the presence of lead as pollutant, is the fact that it has been shown there are distinct LMCT transitions in the UV that are sensitive both to the electronic environment (in this case benzene or toluene) and to the molecular geometry (conformers adopted by two toluene molecules) that accommodates Pb(II). Of particular significance, is the observation that the addition of a methyl group makes quite a profound difference to the nature of the UV spectrum; in this case making a range of $\pi \rightarrow$ Pb (6p) transitions energetically more accessible. Unlike previous assignments of UV spectra,[29] there does not appear to be any evidence for electrons in the Pb(II) 6s orbital being involved in any of the electronic transitions identified in this study.

APPENDIX: SPIN CONTAMINATION IN OPEN-SHELL EXCITED STATES

Adiabatic TDDFT is a single excitation theory and neglects additional roots stemming from the interaction between single and double excitations.[49,50] Spin contamination is the extent to which the calculated $\langle \hat{S}^2 \rangle$ differs from the expected eigenvalue of the same operator. Spin contamination in open-shell excited states results from the absence of double- or higher-excitations needed to correctly describe spin-permuted configurations.[51]

The types of excitation arising from a doublet ground state, such as that of [Pb(benzene)]$^+$, can be categorised into 3 types[50–52] (see Figure 8). Type I and type II excitations involve the singly occupied molecular orbital (SOMO) and can represent proper spectroscopic states as they are clearly doublets and well described by a single excitation theory. However, the type III excitations give states, as single determinants, which are not in themselves eigenfunctions of the spin operator $\hat{S}^2$; spin-adapted configurations are required. The spin-adapted linear combinations of the M$_S = +1/2$ configuration state functions arising from "three electrons in three orbitals" (shown in Figure 8) are constructed using the S$_3$ symmetry group which is isomorphic to C$_{3v}$. From the three determinants, a quartet (S = 3/2) and two doublets (S = 1/2) each with M$_S = +1/2$ arise,

$$\psi_Q = \frac{1}{\sqrt{3}}(|\bar{i}sa\rangle + |is\bar{a}\rangle + |i\bar{s}a\rangle),$$

$$\psi_{D_1} = \frac{1}{\sqrt{2}}(|\bar{i}sa\rangle - |is\bar{a}\rangle),$$

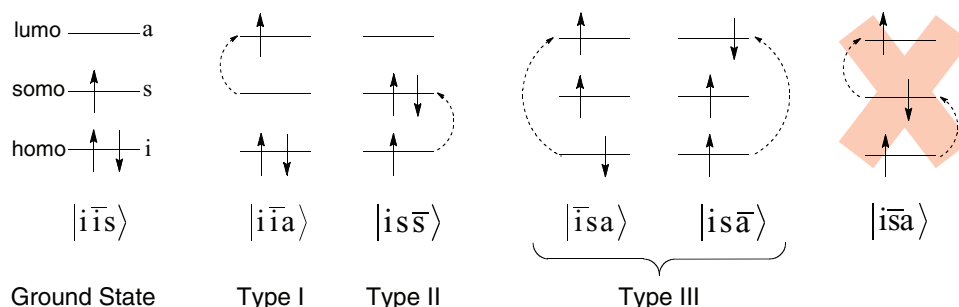$$\psi_{D_2} = \frac{1}{\sqrt{6}}(|\bar{i}sa\rangle + |is\bar{a}\rangle - 2|i\bar{s}a\rangle).$$

FIG. 8. The types of excitation arising from a doublet ground state, where i represents a doubly occupied orbital, s represents the singly occupied orbital, and *a* represents an unoccupied orbital. The presence or absence of a bar over i, s or *a* indicates a beta or alpha spin electron, respectively.

TABLE VII. The excited state spin contamination in each of the [Pb(X)]$^+$ excited states, calculated assuming that all spin contamination comes from the next highest allowed spin component. Heavily spin contaminated states are shown in bold.

	E (cm^{-1})	$\langle \hat{S}^2 \rangle$	$\Delta \langle \hat{S}^2 \rangle$	Doublet character (%)	Spin contamination (%)
[Pb(benzene)]$^+$	38 990	1.00	0.25	91.8	8.2
	41 050	**1.89**	**1.14**	**61.9**	**38.1**
	42 038	0.77	0.02	99.3	0.7
	47 680	0.76	0.01	99.7	0.3
[Pb(toluene)]$^+$	35 244	1.03	0.28	90.7	9.3
	38 098	1.04	0.29	90.3	9.7
	39 663	**1.69**	**0.94**	**68.7**	**31.3**
	41 111	0.77	0.02	99.3	0.7
	44 517	**1.31**	**0.56**	**81.3**	**18.7**
	44 966	**2.14**	**1.39**	**53.7**	**46.3**
	47 397	0.77	0.02	99.3	0.7

Since ordinary TDDFT cannot flip spins, only singlet-coupled: $\frac{1}{\sqrt{2}}(|\bar{i}sa\rangle - |is\bar{a}\rangle)$ and triplet-coupled: $\frac{1}{\sqrt{2}}(|\bar{i}sa\rangle + |is\bar{a}\rangle)$ excitations may occur,[51] however, only the singlet-coupled state ψ_{D_1} is a true eigenfunction of the spin operator. ψ_{D_2} cannot occur in adiabatic TDDFT because of the presence of the configuration $|i\bar{s}a\rangle$ which requires a spin-flip or a double excitation, instead the unphysical triplet-coupled excitation $\frac{1}{\sqrt{2}}(|\bar{i}sa\rangle + |is\bar{a}\rangle)$ is found. Fortunately, Ipatov, Casida *et al.*,[51] have recently provided a formula for determining excited state spin contamination in spin unrestricted TDDFT calculations and this has been implemented in GAUSSIAN 09. For a doublet system, the value should be 0.75. Clearly, several of the values presented in this paper (Tables IV and VI) are severely spin contaminated and should ideally be discarded.

Following Ipatov, Casida *et al.*,[51] and assuming that the quartet state ($S(S + 1) = 3.75$) constitutes the primary source of contamination in the cations, i.e.,

$$|PbX^+\rangle = C_D|doublet\rangle + C_Q|quartet\rangle \text{ so that}$$

$$\langle \hat{S}^2_{calc} \rangle = 0.75|C_D|^2 + 3.75|C_Q|^2,$$

the percentage doublet character in the Kohn-Sham wave function for each of the open shell excited states can be calculated, see Table VII. The [Pb(benzene)]$^+$ excitations at 42 038 and 47 680 cm^{-1} are >99% doublet in character and so in the present work it is safe to classify these states as primarily doublet in character. Similarly, for the [Pb(toluene)]$^+$ states at 41 111 and 47 397 cm^{-1}. However,

it is clear that the [Pb(benzene)]$^+$ excitation at 41 050 cm^{-1} and the [Pb(toluene)]$^+$ states at 39 663, 44 517, and 44 966 cm^{-1} are severely spin contaminated with $\Delta \langle \hat{S}^2 \rangle \approx 1$ which corresponds to states which are too spin contaminated to be considered further as they are ill-defined (i.e., not singlet- or triplet-coupled TDDFT excitations, the latter would result in $\Delta \langle \hat{S}^2 \rangle \approx 2$) and unphysical. They should all be discarded. Finally, the validity of the remaining states for which $\Delta \langle \hat{S}^2 \rangle \approx 0.3$ is more questionable; by assuming that all spin contamination comes from the next highest allowed spin component they are $\approx$90% doublet in character, and so an excitation in this region is likely.

To further analyse this problem, the TDDFT electronic excitation energies of [Pb(benzene)]$^+$ (Figure 6 and Table IV, main text) are presented in Figure 9 along with the nature of the orbitals involved in the most dominant transitions. Here, we have assumed same orbitals with different spins (SODS) but in fact the calculations are performed using different orbitals for different spins (DODS). It would appear from this analysis that the excitation at 42 038 cm^{-1} is reliable; it is a type I excitation. The excitation at 38 990 cm^{-1} is predominantly type II but with some type III, which is reflected in the deviations of $\langle \hat{S}^2 \rangle$ from the true value of 0.75. The excitation at 41 050 cm^{-1} with an $\langle \hat{S}^2 \rangle$ value close to 2 involves some unphysical triplet-coupled excitation and should be discarded. The excitation at 47 680 cm^{-1} is not significantly spin contaminated and can be assumed to arise from the physical singlet-coupled excitation; this is interesting as it indicates that a simple transition orbital analysis is not sufficient to
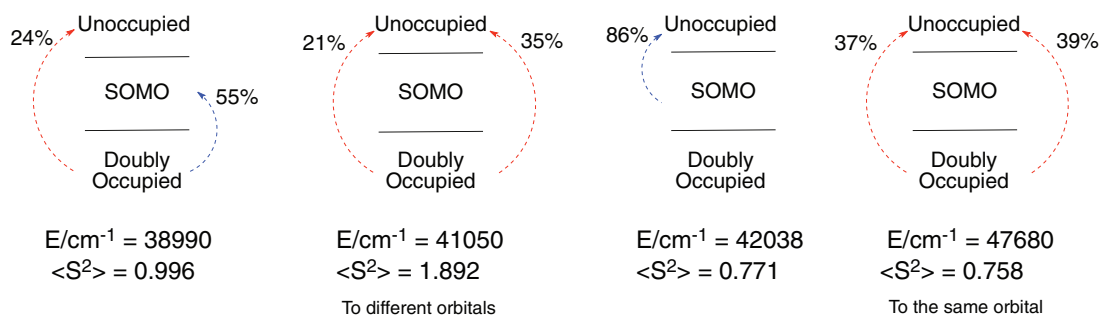
FIG. 9. Analysis of the TDDFT excitations arising from the [Pb(benzene)]$^+$ complex.

distinguish between the unphysical and physical type III excitations of the second and fourth excitations in Figure 9 (and Figure 6). This demonstrates the importance for popular computational quantum chemistry codes to implement the calculation of the $\langle \hat{S}^2 \rangle$ value of excited states, as set out by Casida and co-workers.[51]

In summary, all of the excitations presented for the $[Pb(X)_2]^{2+}$ complexes, X = benzene and toluene, (Tables III and V) are unproblematic as these arise from closed-shell complexes. In the case of the $[Pb(X)]^+$ complexes (Tables IV and VI), any states for which $\langle \hat{S}^2 \rangle$ is not approximately 0.75 should ideally be discarded, in particular the second excitation of the $[Pb(benzene)]^+$ complex and the third, fifth, and sixth excitations of the $[Pb(toluene)]^+$ complex are severely spin-contaminated. However, it should be noted that for $[Pb(toluene)]^+$ (Table VI) the strong transition at 41 111 cm^{-1}, which is a close match to the unassigned experimental feature, is not spin contaminated.

[1] G. Arena, A. Contino, E. Longo, D. Sciotto, and G. Spoto, J. Chem. Soc., Perkin Trans. 2 2287 (2001).

[2] J. Sanchiz, P. Esparza, D. Villagra, S. Dominguez, A. Mederos, F. Brito, L. Araujo, A. Sánchez, and J. M. Arrieta, Inorg. Chem. **41**, 6048 (2002).

[3] Y. Zhang and J. Jiang, J. Phys. Chem. A **113**, 12179 (2009).

[4] C. Lapouge and J. P. Cornard, J. Phys. Chem. **109**, 6752 (2005).

[5] F. Cuenot, M. Meyer, E. Espinosa, and R. Guilard, Inorg. Chem. **44**, 7895 (2005).

[6] D. Bátka and E. Farkas, J. Inorg. Biochem. **100**, 27 (2006).

[7] D. G. Beak, N. T. Basta, K. G. Scheckel, and S. J. Traina, Environ. Sci. Technol. **42**, 779 (2008).

[8] J. P. Cornard, C. Lapouge, L. Dangleterre, and C. Allet-Bodelot, J. Phys. Chem. **112**, 12475 (2008).

[9] J. C. Payne, M. A. ter Horst, and H. A. Godwin, J. Am. Chem. Soc. **121**, 6850 (1999).

[10] A. A. Jarzęcki, Inorg. Chem. **46**, 7509 (2007).

[11] R. S. Brown, B. E. Hingerty, J. C. Dewan, and A. Klug, Nature (London) **303**, 543 (1983).

[12] R. S. Brown, J. C. Dewan, and A. Klug, Biochemistry **24**, 4785 (1985).

[13] G. D. C. Aitken, H. Cox, and A. J. Stace, J. Phys. Chem. A **116**, 3035 (2012).

[14] J. Y. Kwon, Y. J. Jang, Y. L. Lee, K. M. Kim, M. S. Seo, W. Nam, and J. Yoon, J. Am. Chem. Soc. **127**, 10107 (2005).

[15] A. B. P. Lever, *Inorganic Electronic Spectroscopy* (Elsevier, Amsterdam, 1984).

[16] M. A. Duncan, Annu. Rev. Phys. Chem. **48**, 69 (1997).

[17] A. J. Stace, J. Phys. Chem. A **106**, 7993 (2002).

[18] G. Wu, D. Chapman, and A. J. Stace, Int. J. Mass Spectrom. **262**, 211 (2007).

[19] J. Guan, L. Puskar, R. O. Esplugas, H. Cox, and A. J. Stace, J. Chem. Phys. **127**, 064311 (2007).

[20] G. Wu, C. Norris, H. Stewart, H. Cox, and A. J. Stace, Chem. Commun. **2008**, 4153.

[21] G. Wu, H. Stewart, F. D. Lemon, H. Cox, and A. J. Stace, Mol. Phys. **108**, 1199 (2010).

[22] H. Stewart, G. Wu, L. Ma, M. Barclay, A. D. Vieira, A. King, H. Cox, and A. J. Stace, J. Phys. Chem. A **115**, 6948 (2011).

[23] J. T. O'Brien and E. R. Williams, J. Phys. Chem. A **112**, 5893 (2008).

[24] M. F. Bush, R. J. Saykally, and E. R. Williams, ChemPhysChem **8**, 2245 (2007).

[25] T. E. Cooper, J. T. O'Brien, E. R. Williams, and P. B. Armentrout, J. Phys. Chem. A **114**, 12646 (2010).

[26] J. T. O'Brien, J. S. Prell, J. D. Steill, J. Oomens, and E. J. Williams, J. Phys. Chem. A **112**, 10823 (2008).

[27] R. C. Dunbar, J. D. Steill, N. C. Polfer, and J. Oomens, J. Phys. Chem. A **113**, 845 (2009).

[28] R. C. Dunbar, A. C. Hopkinson, J. Oomens, C.-K. Siu, K. W. M. Siu, J. D. Steill, U. H. Verkerk, and J. Zhao, J. Phys. Chem. B **113**, 10403 (2009).

[29] E. S. Claudio, H. A. Godwin, and J. S. Magyar, Prog. Inorg. Chem. **51**, 1 (2003).

[30] G. Bauer, G. S. Nikolov, and N. Trendafilova, J. Mol. Struct. **415**, 123 (1997).

[31] Y. Zhang, X. Zhang, Z. Liu, Y. Bian, and J. Jiang, J. Phys. Chem. A **109**, 6363 (2005).

[32] J. P. Cornard and C. Lapouge, Chem. Phys. Lett. **438**, 41 (2007).

[33] J. P. Cornard, L. Dangleterre, and C. Lapouge, J. Phys. Chem. A **109**, 10044 (2005).

[34] L. Puskar, P. E. Barran, B. J. Duncombe, D. Chapman, and A. J. Stace, J. Phys. Chem. **109**, 273 (2005).

[35] L. Puskar, H. Cox, A. Goren, G. D. C. Aitken, and A. J. Stace, Faraday Discuss. **124**, 259 (2003).

[36] M. J. Frisch, G. W. Trucks, H. B. Schlegel *et al.*, GAUSSIAN 09, Revision A.02, Gaussian, Inc., Wallingford, CT, 2009.

[37] S. H. Vosko, L. Wilk, and M. Nusair, Can. J. Phys. **58**, 1200 (1980).

[38] A. D. Becke, Phys. Rev. A **38**, 3098 (1988).

[39] J. P. Perdew, Phys. Rev. B **33**, 8822 (1986).

[40] J. Tao, J. P. Perdew, V. N. Staroverov, and G. E. Scuseria, Phys. Rev. Lett. **91**, 146401 (2003).

[41] C. Adamo and V. Barone, J. Chem. Phys. **110**, 6158 (1999); J. P. Perdew, K. Burke, and M. Ernzerhof, Phys. Rev. Lett. **77**, 3865 (1996); **78**, 1396 (1997).

[42] See http://www.theochem.uni-stuttgart.de for details of the energy-consistent pseudopotential for Pb; W. Kuechle, M. Dolg, H. Stoll, and H. Preuss, Mol. Phys. **74**, 1245 (1991).

[43] T. Yanai, D. P. Tew, and N. C. Handy, Chem. Phys. Lett. **393**, 51 (2004).

[44] R. L. Martin, J. Chem. Phys. **118**, 4775 (2003).

[45] See supplementary material at http://dx.doi.org/10.1063/1.4801440 for further details.

[46] The eclipsed-cis structures calculated using the hybrid functionals TPSSh and PBE0 functional have a small imaginary mode (3i cm^{-1}). Distorting along this mode resulted in the staggered-cis conformation. However, for BPV86 the C_{2v} eclipsed-cis structure was a true minimum. The TPSSh energy in Table II is calculated using the symmetry-constrained C_{2v} structure.

[47] R. L. Davidovich, V. Stavila, D. V. Marinin, E. I. Voit, and K. H. Whitmire, Coord. Chem. Rev. **253**, 1316 (2009); M. Kaupp and P. v. R. Schleyer, J. Am. Chem. Soc. **115**, 1061 (1993); L. Shimoni-Livny, J. P. Glusker, and C. W. Bock, Inorg. Chem. **37**, 1853 (1998).

[48] J. Jingang, L. Puskar, G. Akibo-Betts, H. Cox, and A. J. Stace, "Experimental and theoretical study of the photofragmentation spectra of Pb(benzene)$n+$ complexes, $n = 1$-5" (unpublished).

[49] D. Maurice and M. J. Head-Gordon, Phys. Chem. **100**, 6131 (1996).

[50] Z. Rinkevicius, I. Tunell, P. Salek, O. Vahtras, and H. Ågren, J. Chem. Phys. **119**, 34 (2003).

[51] A. Ipatov, F. Cordova, L. J. Doriol, and M. E. Casida, J. Mol. Struct.: THEOCHEM **914**, 60 (2009).

[52] P. T. van Duijnen, S. N. Greene, and N. G. J. Richards, J. Chem. Phys. **127**, 045105 (2007).